

Holocene Dune Activity in the Thar Desert, India

Aayush Srivastava^{1*}, David S.G. Thomas^{1, 2} and Julie A. Durcan¹

¹ School of Geography and the Environment, University of Oxford, Oxford, OX1 3QY, United Kingdom

² School of Geography, Archaeology and Environmental Studies, University of the Witwatersrand, Johannesburg 2050, South Africa

*Correspondence to: aayush.srivastava@ouce.ox.ac.uk

Abstract

The Thar Desert dune system in north-west India and eastern Pakistan provides a rich archive of past environmental, geomorphological and climatic change. Much of the knowledge about the timing of dune accumulation in the Thar stems from scattered and sporadic records, based on older luminescence dating protocols. If the Thar dune record is to be incorporated within a growing multiproxy framework of past climate and environmental dynamics, it is necessary to generate a systematic record of the timing of dunefield accumulation. From this, relationships to climate and other drivers of dune activity may then be better established. To this end, an intensive programme of field sampling and optically stimulated luminescence (OSL) dating was carried out from a dunefield in the east-central Thar Desert. This study presents the first detailed Holocene dune accumulation history from the region, and sheds light on the development of the multi-generational parabolic dune systems. In contrast to previously published work, we identify the importance of the Holocene and the last millennium as periods with a number of preserved accumulation phases. OSL ages suggest that accumulation was persistent during the early and mid-Holocene (within 11.7- 5.5 ka), late Holocene (2-1 ka), as well as two major phases in the last millennium (600 – 200 a and within the last 70 a). Potential drivers of dune mobility in the last century include a strong anthropogenic dimension. Rapid net accumulation is recorded in the last 70 years, with rates varying between 2 and 5 m/ year, in an environment where agricultural pressures have increased dramatically with the advent of irrigation schemes expanding into dunefield areas.

Keywords: Thar Desert, optically stimulated luminescence (OSL) dating, parabolic dunes, Holocene, geomorphological change.

1 Introduction

The Thar Desert forms an integral part of the arid lands of western India and eastern Pakistan, between the Aravalli hills in the east and the Indus plains to the west. The desert is often considered as the easternmost extension of the vast Saharo-Arabian subtropical desert belt (Singhvi and Kar 2004; Roy et al., 2009), and is dominated by aeolian bedforms of various dimensions and forms. Many sand dune types have been identified in the region, including parabolic, transverse, linear, star and network dunes

(Figure 1) (Wasson et al., 1983; Kar 1993). The desert is located in a transitional but dominant south-west monsoon regime, which not only controls wind seasonality, precipitation and vegetation cover, but also implies that minor perturbations in monsoon dynamics may impact the geomorphic processes, including aeolian dynamics, in this seasonally semi-arid to arid region. The extensive dune systems in the Thar therefore provide an opportunity to understand temporal changes in aeolian dynamics during the late Quaternary.

The first application of luminescence dating to aeolian sands anywhere occurred in the Thar Desert (Singhvi et al., 1982), and this seminal study inspired a move from qualitative assessments of long term dune accumulation histories to temporally specific records. The Thar was one of the leading deserts in luminescence dating applications to aeolian sediments, and in the 35 years since this first application, numerous dune sites have been dated in the region (e.g. Chawla et al., 1992; Singhvi et al., 1994; Kar et al., 1998; Thomas et al., 1999), with dated records used to address the long-standing debate surrounding the potentially recent anthropogenic origins of the Thar Desert, as suggested in early studies by Piggot (1950) and Bryson and Barreis (1967). However, the sampling and dating strategies employed in earlier luminescence dating studies focussed largely on accessing deep trenches in basal sediments, often associated with the expansion of irrigation canals into the region, for establishing the antiquity of aeolian episodes and finding major phases of dune accumulations (Kar, 2013; Dhir et al., 2010). More recent studies have tended to focus on the desert margins, within the context of aeolian-fluvial interactions (e.g. Juyal et al., 2006; Saini et al., 2009; Saini and Mujtaba., 2012; Giosan et al., 2012; Shitaoka et al., 2012; Durcan et al., 2017).

To date, the application of systematic and intensive dunefield sampling programmes has been less prevalent in the Thar than in other deserts, such as the Kalahari in Africa (Stone and Thomas, 2008), the Rub' al Khali in Arabia (Leighton et al., 2013; Atkinson et al., 2011) and the Strzelecki and Tirari in Australia (Fitzsimmons et al., 2007). In the Thar, the focus on deeper sequences has potentially resulted in a bias towards older accumulation phases, with relatively younger accumulation phases not sampled. Singhvi and Kar (2004) note that existing data sets provide little opportunity to understand the impact of climate and humans on desert evolution and geomorphological processes during the late Holocene. Interrogation of existing geochronological data is also hampered by a common absence of detailed locational and sampling depth data within published records. In addition, all 146 luminescence ages from the Thar Desert dune systems listed in INQUA Dune Atlas chronologic database (Lancaster et al., 2016) utilised multiple aliquot protocols, which are associated with relatively large age uncertainties (e.g. Stokes, 1994). Both instrumental and methodological advances in luminescence dating, including the single aliquot regenerative (SAR) dose protocol (e.g. Murray and Wintle, 2000, 2003; Wintle and Murray, 2006) and single grain luminescence dating (e.g. Duller et al., 2003, 2008) provide the potential for more robust age calculation. In the context of geochronological improvements, and rapid anthropogenic land clearance and disturbance in the Thar Desert, conducting a systematic analysis of Thar dune accumulations chronologies becomes an important research priority. Therefore, the

aim of this paper is to present new dune accumulation records from the Thar Desert, following intensive sampling and the application of modern luminescence dating protocols, and to assess spatial variability within a dunefield. This study allows a more temporally-complete assessment of the region's dune accumulation history and provides an insight into the dune evolution in this arid to semi-arid dryland zone.

2 Study Site and Methodology

The aeolian landforms in the Thar are dominated by various types of dunes which cover ~50% of the region (Kar et al., 1993; Moharana et al., 2013), the majority of which occur in western Rajasthan, India (Figure 1) and adjoining parts in Pakistan. The present study focusses on the Shergarh-Dechu region in the Arid Western Plain of the central Thar, which is dominated by parabolic dunes. These parabolic dunes form a clustered 'rake-like' appearance (Figure 2A), with longer arms in the middle of the parabolic cluster and gradually shorter arms on each side. The arms can be up to 2500 m long, with inter-arm spacing ranging between 150 m and 650 m. These 'rake-like' parabolic dunes have rounded nose which contains more than 35% sand volume in the dunes (Kar et al., 2004). The Shergarh-Dechu region is classified as arid to semi-arid, with mean annual precipitation typically varying between 250 – 400 mm where dunes are relatively stable under natural conditions. In the present-day conditions, winds in the region increase in strength from March onward, peaking in June and decline after the arrival of monsoonal precipitation in July. This context provides an ideal location for examining the timing and amplitude of spatial changes in aeolian activity in the past and its correlation with variations in monsoonal precipitation.

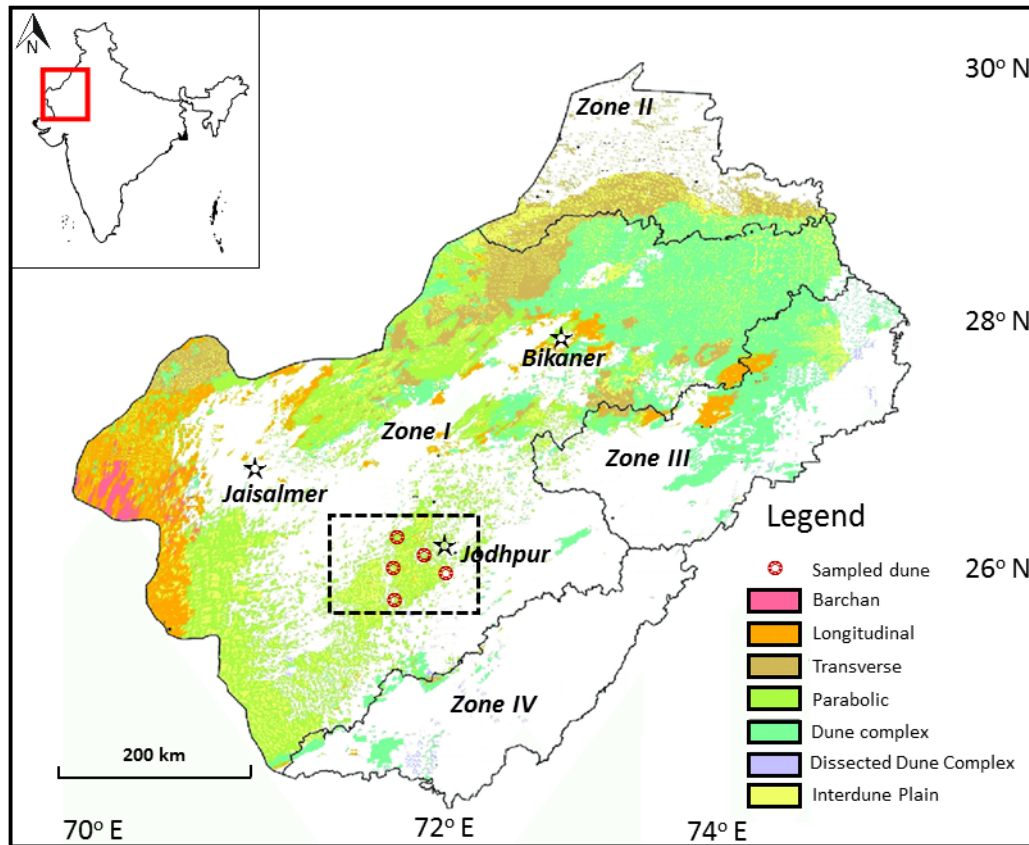


Figure 1. Based on climate and land use pattern indices, the Thar is divided into four zones, namely Arid Western Plain (Zone 1; 133073 sq. km), Irrigated North-Western Plain (Zone 2; 20557 sq. km), Transitional Plains of Inland Drainage Basin (Zone 3; 31329 sq. km) and Transitional Plains of Luni Basin (Zone 4; 22951 sq. km). The dotted box shows the Shergarh-Dechu region in Zone 1 with the location of five sampled dune sites (red wheels) and major cities (stars) (Figure modified from Moharana et al., 2013).

2.1 Site Selection and Sampling

Five dunes sites (Tinwari, Shergarh, Setrawa, Chamu and Dechu) were sampled to test the spatial variability of dune accumulation histories within the dunefield (Figure 2A). Samples were collected from vertical sections, by carefully cutting steps through the nose and arms of the dunes using hydraulic diggers (Figure 2B, C). At Tinwari site, samples were collected from the 23 m deep section located in the nose of the dune (Thar 16/1, Thar 16/3). Four samples were collected from the dune arm from a 2 m deep pit, situated 500 m from the dune nose (Thar 18/1). Similarly, at Setrawa samples were collected from a 7 m deep section located in the nose of the dune (Thar 16/6) and another 7 m section from a section in the dune arm, located ~600 m from the nose (Thar 18/2). The samples from dune arms generated very young ages with indiscernible OSL signal sometimes, therefore, at Shergarh (Thar 16/4), Chamu (Thar 16/9) and Dechu (Thar 16/10), samples were collected from 9.0 m, 8.5 m and 10.2 m deep sections respectively, all located near the nose of the dune only. The sediment faces of dug sections were cleaned prior to sampling. Samples were collected by hammering black light tight tubes into the cleared sediment face, and a resolution of 1.0 m interval was adopted where possible taking into account accessibility and sediment collapse risks, with additional sampling carried out to bracket the fine bedding structures observed at the top of the dunes.

2.2 Sedimentological Analyses

Grain size analyses were conducted using a Malvern Mastersizer Hydro 2000 laser grain analyser and analysed using Gradistat (Blott, 2000) following the method of Folk and Ward (1957). Colour analysis was conducted on oven-dried samples using a Munsell colour chart. Organic and carbonate contents were determined by heating the sediment to 550° C and 950° C respectively, following the process outlined in Heiri et al. (2001).

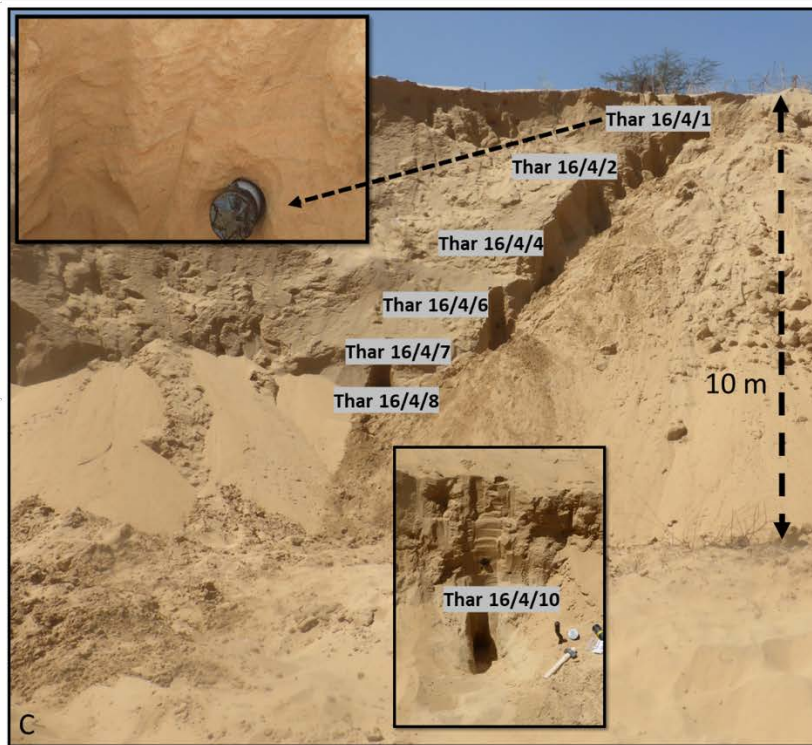
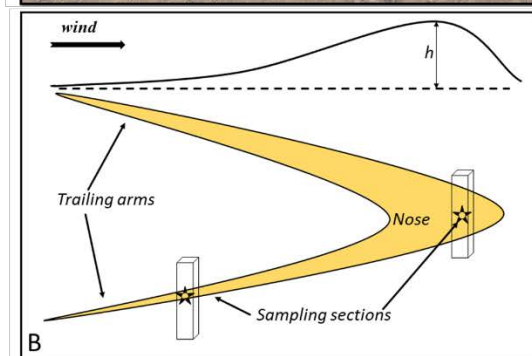
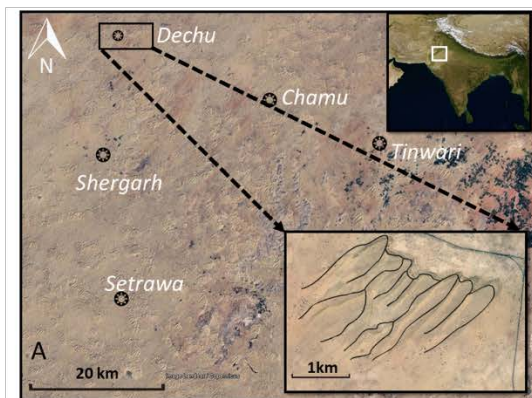
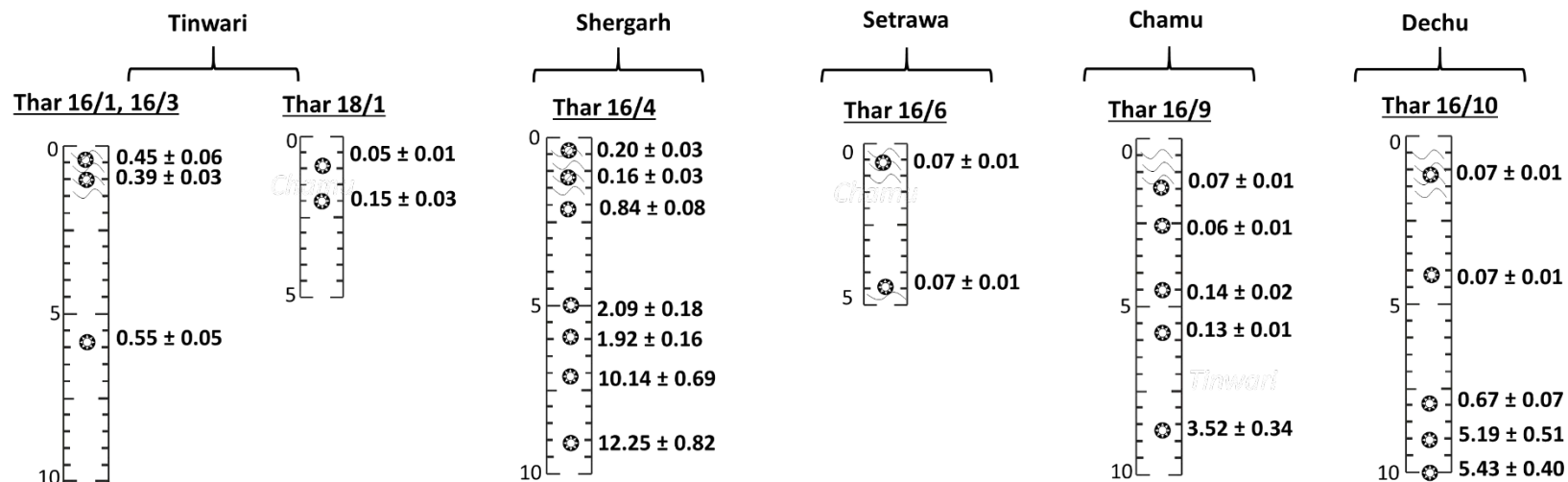
2.3 Luminescence Dating

Samples were opened in subdued orange-light conditions in the Oxford Luminescence Dating Laboratory, University of Oxford. The light-exposed sample ends were removed and used for sedimentological analyses and measurement of radionuclide concentrations. Sediments were treated with hydrochloric acid and hydrogen peroxide to remove carbonate and organic matter, and were sieved to isolate the 180-210 µm grain size fraction. Quartz mineral grains were isolated by heavy liquid (sodium polytungstate) density separation. Hydrofluoric acid was used to remove the alpha-irradiated outer surface of the quartz grains. Initial tests indicated feldspar contamination, and therefore samples were treated with fluorosilicic acid for two weeks to reduce persistent feldspar contamination. Sediments were treated with hydrochloric acid after each chemical etch to remove any fluoride precipitate, prior to re-sieving.

OSL measurements were made using Risø DA-15 TL/OSL readers (Bøtter-Jensen et al., 2003), fitted with either blue (470 nm) or green (525 nm) LEDs and $^{90}\text{Sr}/^{90}\text{Y}$ beta sources with dose rates varying between 3.5 and 4 Gy/minute. Luminescence signals were detected through a bi-alkali photomultiplier tube, fitted with 7.5 mm Hoya U-340 filters. A post-IR blue SAR protocol (Banerjee et al., 2001; Murray and Wintle, 2000) was used to calculate equivalent doses (D_e) as a further precaution against any residual feldspar contamination. Following pre-heat plateau and dose recovery tests, a pre-heat of 240° C for 10 seconds and a cut-heat of 160° C for 0 s were selected for use. Samples were stimulated with infra-red light (870 nm) at 50° C for 100 s, prior to measurement of the blue/green stimulated luminescence at 125° C for 40 s. Sediment was adhered to aluminium discs using silicon spray and small aliquots were used for all but three samples. Small aliquots had a diameter of 2 mm (~70 grains per disc), medium had a 5 mm diameter (~425 grains) and large aliquots an 8 mm (~1100 grains) (e.g. Heer et al., 2012). Single grain analyses were done on four samples, Thar 16/1/9, 16/4/2, 16/4/10 and 16/10/10, to establish the number of luminescence grains giving light in response to a laboratory beta dose. 500 grains of each of these samples were given a 50 Gy dose and the number of grains giving a luminescence signal discernible above machine background were counted.

Luminescence signals were screened using a standard set of rejection criteria (e.g. Jacobs et al., 2006). Signals were included in D_e calculation when 1) recuperation was either less than 5% (where sample D_e was greater than 1.5 Gy) or 0.25 Gy (for D_e s less than 1.5 Gy); 2) the recycling ratio was within 10% of unity including uncertainties (Murray and Wintle, 2003); and 3) test dose signal were at least 3σ greater than the background. Final D_e determinations were calculated using the central age model (CAM) of Galbraith et al. (1999), using the R Luminescence package (Kreutzer et al., 2017). In addition, dose recovery tests were carried out on samples Thar 16/1/2, Thar 16/1/7, Thar 16/3/2, Thar 16/4/4, Thar 16/6/1, Thar 16/9/4 and Thar 16/10/10, which provided dose recovery ratios of 0.95 ± 0.05 , 0.93 ± 0.06 , 0.94 ± 0.07 , 0.99 ± 0.06 , 1.0 ± 0.10 , 0.97 ± 0.07 , 0.98 ± 0.10 respectively, indicating that the post-IR blue SAR protocol, analyses and methods used for D_e determination can successfully recover an applied laboratory dose.

Environmental dose rates were calculated from radionuclide concentrations measured using inductively coupled plasma mass spectrometry at the Scottish University Environmental Research Centre. Infinite-matrix dose rates were calculated using the conversion factors of Guerin et al. (2011) and were adjusted for attenuation by grain size (Guerin et al., 2012), chemical etching (Bell, 1979) and a moisture content of 5 ± 2 %. The cosmic dose rate was calculated according to Prescott and Hutton (1994), and all dose rates calculations were made using DRAC (v1.2) software of Durcan et al. (2015).

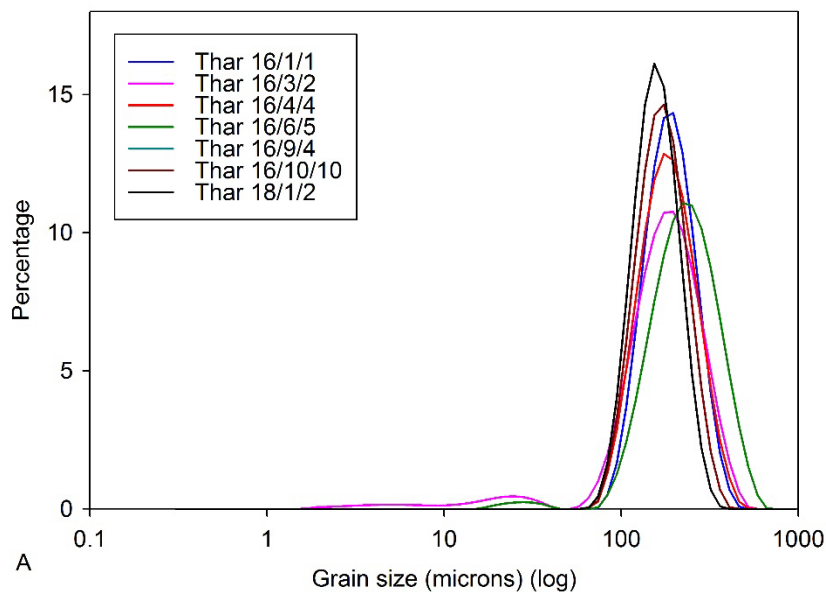


1 **Figure 2. (A) The location of sampled dune sites Tinwari (26.58397 N, 72.81615 E; 26.579361 N, 72.814240 E), Setrawa (26.60192 N,**
2 **72.28866 E; 26.596704 N, 72.285504 E), Shergarh (26.33122 N, 72.28821 E), Dechu (26.81859 N, 72.30316 E) and Chamu (26.66854 N,**
3 **72.57005 E); all of which are located within the arid to semi-arid Shergarh-Dechu region located on the Arid Western Plain. (B). A**
4 **schematic representation of sampling sections within a parabolic dune. (C). An example of the sampled section at Shergarh (Thar 16/4).**
5 **Samples were collected by cutting steps into the dune section to allow access to undisturbed sediment. An offset sample Thar 16/4/10**
6 **offset was collected after calculating the depth profile along the main trench. Inset, an OSL sample tube hammered into the cleared**
7 **sediment face. The presence of laminations demonstrates a lack of post-depositional disturbance. (D) The schematic view of sampled**
8 **sections with OSL ages (ka). Sample depths are in metres. Most sites consisted of homogeneous dune sands, with the exception of**
9 **some weak laminations, which are indicated by the curved lines.**

3 Results

3.1 Sedimentology

All sampled dune sections have a unimodal, dominantly medium to fine sand distribution with mean size varying between ~150 and ~270 μm (Table 1; Figure 3A). Silt component ranges between 0 and 15%, and there is less than 1.1% clay for all samples (Figure 3B). At each site, the upper part of the sampled parabolic crests consists exclusively of unimodal fine sand (for example, samples Thar 16/1/1, 16/1/2, 16/4/1, 16/4/2, 16/9/1, 16/9/2, 16/10/1) with an absence of finer silt and clay (Figure 3B), reflecting proximity to an active dune surface. Samples are negatively skewed, mostly very leptokurtic or mesokurtic, and sorting of the younger sediments varies between moderately well to well sorted (Table 1). The dune sediments are homogenous in colour within each dune, with yellowish brown as the predominant colour (Table 1). Generally, the samples contain 0.5 % to 2.0 % carbonates (by weight), except for some basal units at Tinwari and Shergarh, which have slightly higher contents (~3 %) and are adjacent to underlying pedogenic calcretes. The organic content in the samples is less than 2.0 % by weight (Table 1).



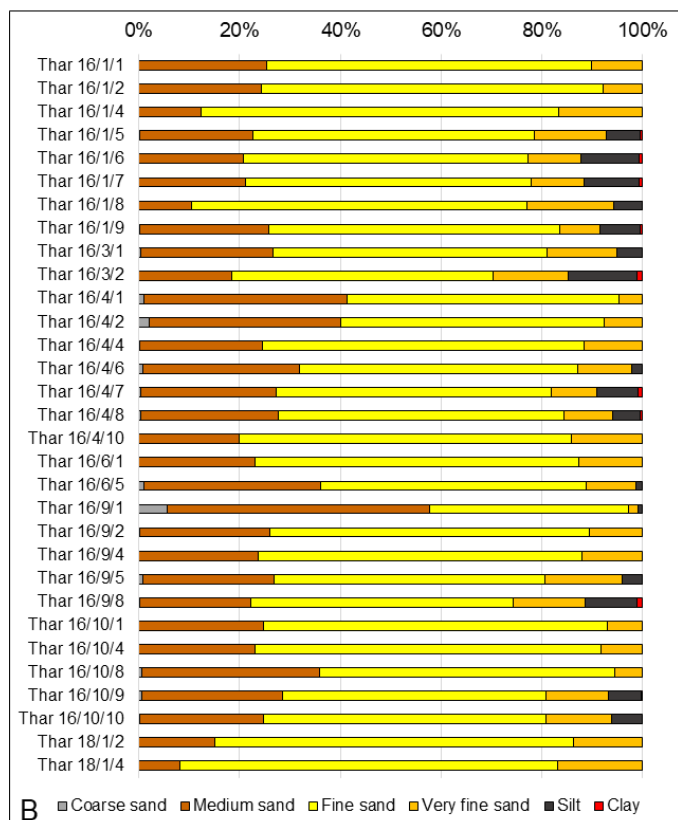


Figure 3. (A) Grain size distribution data for selected samples, and (B) The percentage distribution of different grain sizes for all the samples.

3.2 Luminescence Dating

OSL age data are presented in Table 2 and in Figure 2D. OSL signals from the sample were sufficiently bright to differentiate from machine background levels (Figure 4). Use of the fast ratio (Durcan and Duller, 2011) suggests the dominance of the fast component in the initial part of the OSL signal. Single grain analyses of samples showed that between 2.4 and 4.0 % of measured grains gave a discernible luminescence signal after a 50 Gy dose, suggesting that on average, small aliquots in this study should have 2-3 luminescing grains per disc, medium 10-17 grains, and large 26-45 grains. Therefore, in the presence of very few luminescing grains per multi-grain aliquot, any heterogeneity in dose distributions will be identifiable.

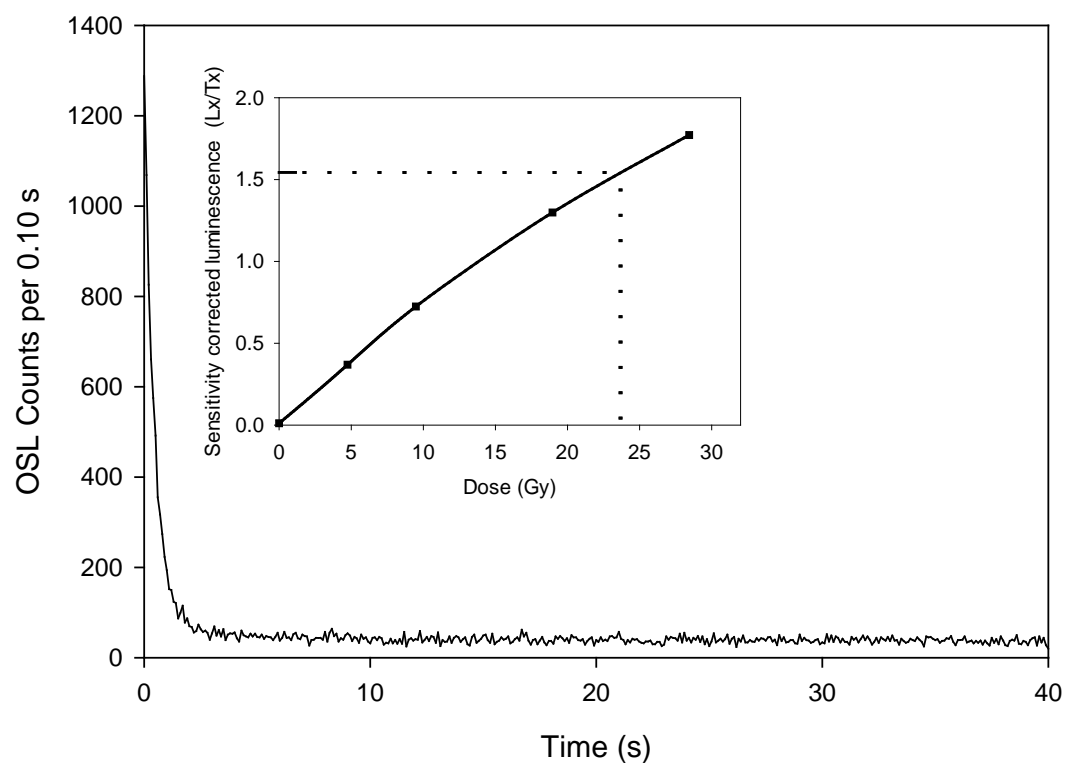


Figure 4. An example of OSL signal from a small aliquot of sample Thar 16/1/8. Inset, corresponding dose response curve fitted using an exponential function.

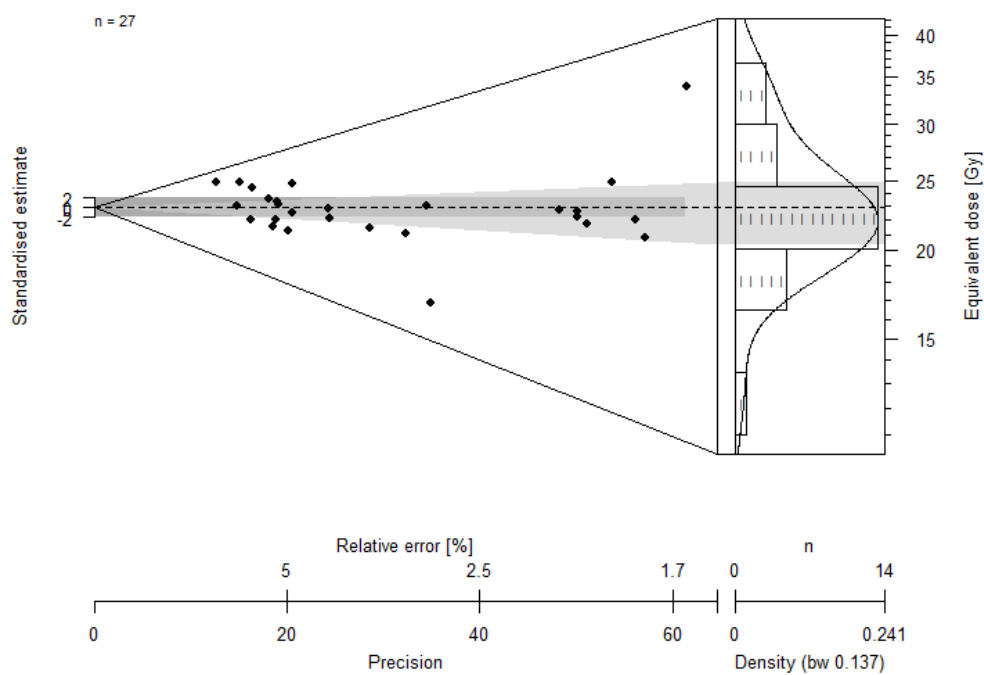


Figure 5. Abanico Plot (plotted using ShinyPlot; Dietze et al., 2016) of individual D_e s of sample Thar 16/4/8. The sample D_e of 22.84 ± 0.91 Gy is shown by the dashed line and $\pm 2\sigma$ by the grey shaded area.

Over-dispersion (σ_d) or heterogeneity in D_e distributions beyond that expected from intrinsic variability, for this suite of ages is relatively low, and ranges between 20 % and 35 % (including uncertainties) for samples with D_e s greater than 1 Gray (Table 2). Variability in D_e distributions can originate from a multitude of factors including partial bleaching of sediments prior to deposition (e.g. Olley et al., 2004), environmental dose rate heterogeneity (e.g. Nathan et al., 2003), and post-depositional mixing like bioturbation (e.g. Bateman et al., 2007). Given the depositional environment in this study, partial bleaching of sediments prior to deposition is unlikely, given the efficiency of bleaching during aeolian transport, and asymmetry in D_e distributions is not observed. Visual evidence for post depositional mixing was not observed during sampling, and undisturbed sediments were targeted for dating (e.g. Figure 2C, inset). Therefore, mild microdosimetric variability is hypothesised (but not confirmed) to explain variability in D_e s. σ_d for young samples (where $D_e < 1$ Gy) is slightly higher (35 – 75 %; Table 2), although this should be expected in the mathematic context of low D_e s providing small denominators, which amplifies σ_d values. Large σ_d values are commonly seen in young samples, and for example, Arnold et al. (2009) report σ_d values up to 208 % for samples less than 350 years of age. For the majority of samples measured in this study, dose distributions vary symmetrically around a central value (e.g. Figure 5), and therefore the central age model of Galbraith et al. (1999), has been selected for use, following the approach of Durcan et al. (in press) and references therein.

The suite of OSL ages in this study presents evidence of a dynamic aeolian environment throughout the Holocene in the east-central part of the Thar Desert. The oldest sample is Thar 16/1/9 at Tinwari, which is the easternmost sample site (Figure 2A), dating to 13.85 ± 1.11 ka at a 23 m depth. For the most part, ages are consistent with depth (within uncertainties), and there is a general trend for phases of large units of up to ~6 m of sediment to accumulate within relatively short periods of time, with more distinctive, older phases recorded at greater depth; for example, at Chamu the upper 5.5 m section accumulated in last 150 years and is underlain by 3.52 ± 0.34 ka old unit (Thar 16/9/8). Likewise, at Tinwari, the upper 6 m dune section accumulated at the rate of ~1 m/century whilst the lower 3 m dune section accumulated at ~0.4 m/ka (Table 2; Figure 6). Several periods of dune accumulation have been identified including at least one site in each dune recording dune activity and accumulation in the last 500 years (Figure 6). The sampled sand dunes at Tinwari (Thar 16/1/1, Thar 16/1/2 and Thar 16/1/4), Shergarh (Thar 16/4/1 and Thar 16/4/2) and Dechu (Thar 16/10/8) all record accumulation between 200 and 600 years, while samples from Setrawa (Thar 16/6/1 and Thar 16/6/5), Chamu (Thar 16/9/1, Thar 16/9/2) and Dechu (Thar 16/10/1 and, Thar 16/10/4) and Tinwari (18/1/2) all provide ages that show the accumulation of 3-4 m of dune sand in second half of twentieth century (0.07 ± 0.01 ka, 0.06 ± 0.01 ka and 0.05 ± 0.01 ka; Figure 6).

4 Discussion

4.1 Holocene dune activity in the region

The oldest OSL ages of 13.85 ± 1.11 ka and 12.25 ± 0.82 ka, observed at Tinwari and Shergarh demonstrate the relative youth of dune bodies in the region. The presence of sparse calcified nodules and plant roots also attest to the greater stability of these dunes (Wasson et al., 1983). Previously published luminescence ages from the Thar, even though with large errors, do not include evidence of dune building during the early Holocene (Singhvi and Kar, 2004; Prasad and Enzel, 2006; Figure 7), yet this had been identified as a period marked by strong south-west monsoon winds based on the enhanced upwelling off the coast of Oman (Gupta et al., 2003; Figure 8). The sites investigated in this study provide evidence of early Holocene aeolian activity and dune building, with sand accumulation ages between 10.14 ± 0.69 ka (Thar 16/4/8) and 9.60 ± 0.74 ka (Thar 16/1/8), and accumulation continuing 6.86 ± 0.49 ka (Thar 16/1/6). The dunes experienced accumulation in the mid-Holocene at ~ 5 ka (Thar 16/3/2, Thar 16/10/9 and Thar 16/101/10) and then at ~ 3.5 ka (Thar 16/9/8). These ages coincide with a period of lower precipitation between 5.0-3.5 ka, as recorded in the annually laminated (varved) marine records of north-eastern Arabian Sea (von Rad et al., 1999; Figure 8).

The east-central part of the Thar Desert was previously thought to have stabilised after ~ 3.5 ka, with more recent dune accumulation confined to the presently arid western Thar (Kar et al., 1998; Thomas et al., 1999). Kar et al. (2004) noted very little trace of dune accumulation from ~ 5 ka onward in the eastern and southern part of the desert. Our data identify widespread late Holocene dune accumulation in the eastern Thar as well (1.92 ± 0.16 ka at Thar 16/4/7 and 1.07 ± 0.09 ka at Thar 16/1/5). Recent studies by Durcan et al. (in press) have also identified dune accumulation in the northern margin of the desert, along the Ghaggar-Hakra palaeochannel, at ~ 1.9 ka and ~ 2.2 ka, linking dune activity with the gradual drying of the fluvial channel. Together, the suite of ages from different regions provides an emerging picture of widespread aeolian accumulation in the late Holocene. Establishing the precise spatial extent of Thar Desert dune activity at this time will require additional new records of dune accumulation timing from further regions in the system.

Thomas et al. (1999) and Singhvi and Kar (2004) noted that existing data sets provide little opportunity to establish whether dune activity had been a feature of recent centuries. Of the previously published luminescence ages from dunes in the region, only one age, from Chamu (Thomas et al., 1999) is from the last one thousand years, and this is a modern age of 0.06 ± 0.01 ka, with others falling predominantly in the 10-100 ka period (Figure 7). By intensively sampling dune profiles, our study has identified at least two recent phases of dune accumulation, between 600 and 200 years ago and very recently, in the last 70 years (Figure 6). It is notable that other precipitation proxy records available for this part of Asia, like the marine core proxy rainfall record of Von Rod et al. (1999) from the Arabian Sea or the oxygen-isotope record from a stalagmite from southern Oman (Fleitmann et al., 2003) identify reduced rainfall 600-200 years ago (Figure 8). Closer to the study area, Singhvi and Kar (2004)

noted that the Luni River, ~100 km distant, did not record any flooding during this period.

The twentieth century ages, recorded in the dunes as a result of preservation bias towards younger sediments (Bailey and Thomas, 2014), indicate the sensitivity of parabolic dunes to environmental disturbances. These ages coincide with India's independence, expansion of irrigational network and mechanised farming in the most arid districts, and the subsequent rise in human population in the desert region, which together have increased the potential for activation of dune sands. Degradation of natural vegetation has been widespread since then, as most of the permanent pasture lands in dunefield areas were very severely exploited for fuelwood and fodder. Uprooting of sand binder shrubs species, like *Calligonum polygonoides* and *Leptadenia pyrotechnica*, to make way for crops, has also aided sand transport (Kar, 2009). Unrestricted over-pumping of groundwater to support both livestock and arable agriculture is resulting in the gradual emptying of aquifers, and increasing salinity in the region (Rodell et al., 2009), which bears a direct implication for the stability of parabolic dunes in the region. The expansion of agriculture including an increase in intensification has been known to reactivate parabolic dunes in Nyírség in Hungary (Kiss et al., 2012) and Horqin sandfields in Inner Mongolia, China (Zhao et al., 2007), and the acceleration of dune accumulation in the last 70 years (Figure 6) suggests that the same has occurred in this part of the Thar Desert.

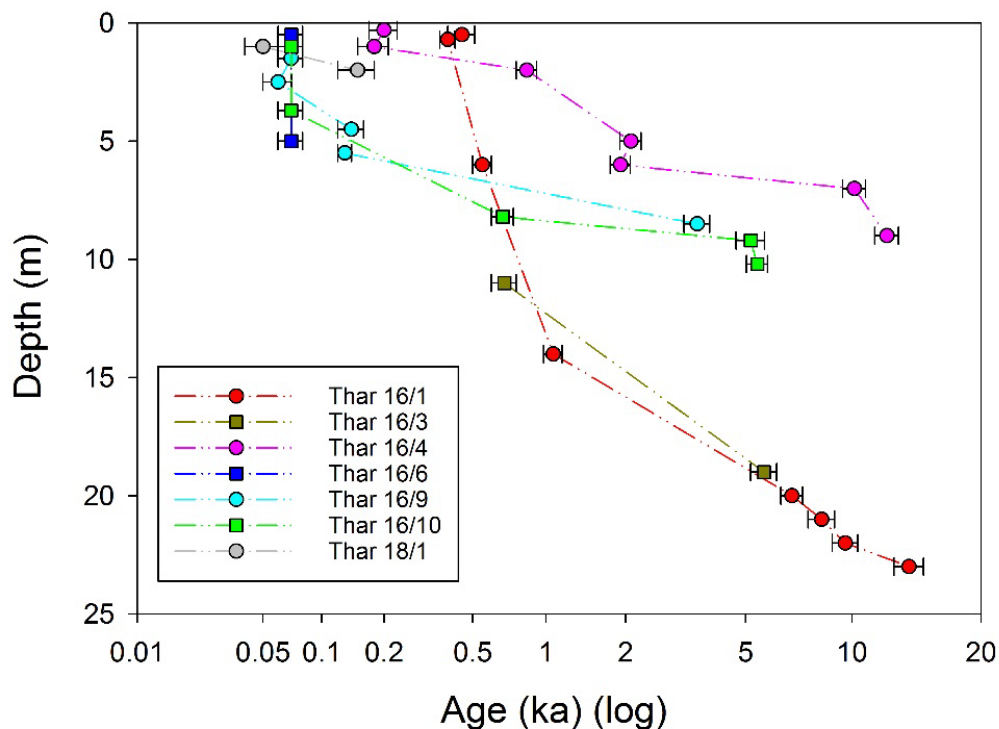


Figure 6. Age-depth plot for the OSL ages presented in Table 2. The steep lines denote the timing of periods of high dune accumulation, for example, Thar 16/1 shows a high accumulation between 500-1000 years ago at the rate of ~1.6 m/century. Likewise, the vertical line of Thar 16/6 shows the rapid accumulation of 5 m of dune 70 years ago.

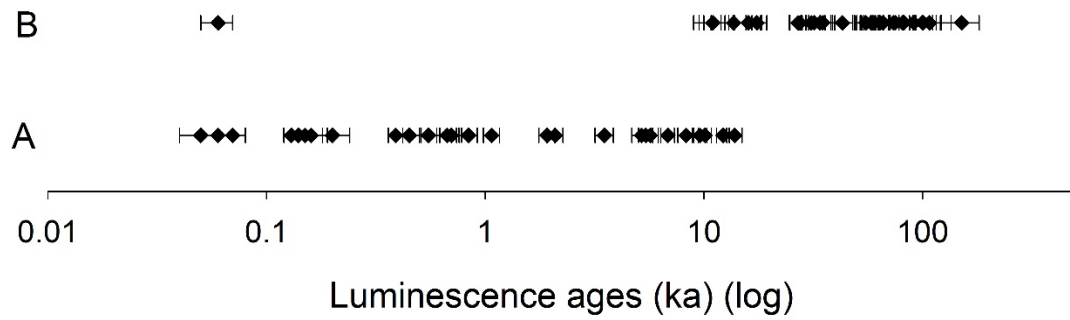


Figure 7. Comparison of the OSL dune age data from this study (A) with the previously published TL and OSL ages (B) from the Shergarh-Dechu basin in the Thar Desert (Thomas et al., 1999 (n=2); Singhvi and Kar, 2004 (n=16); Dhir et al., 2010 (n=13)).

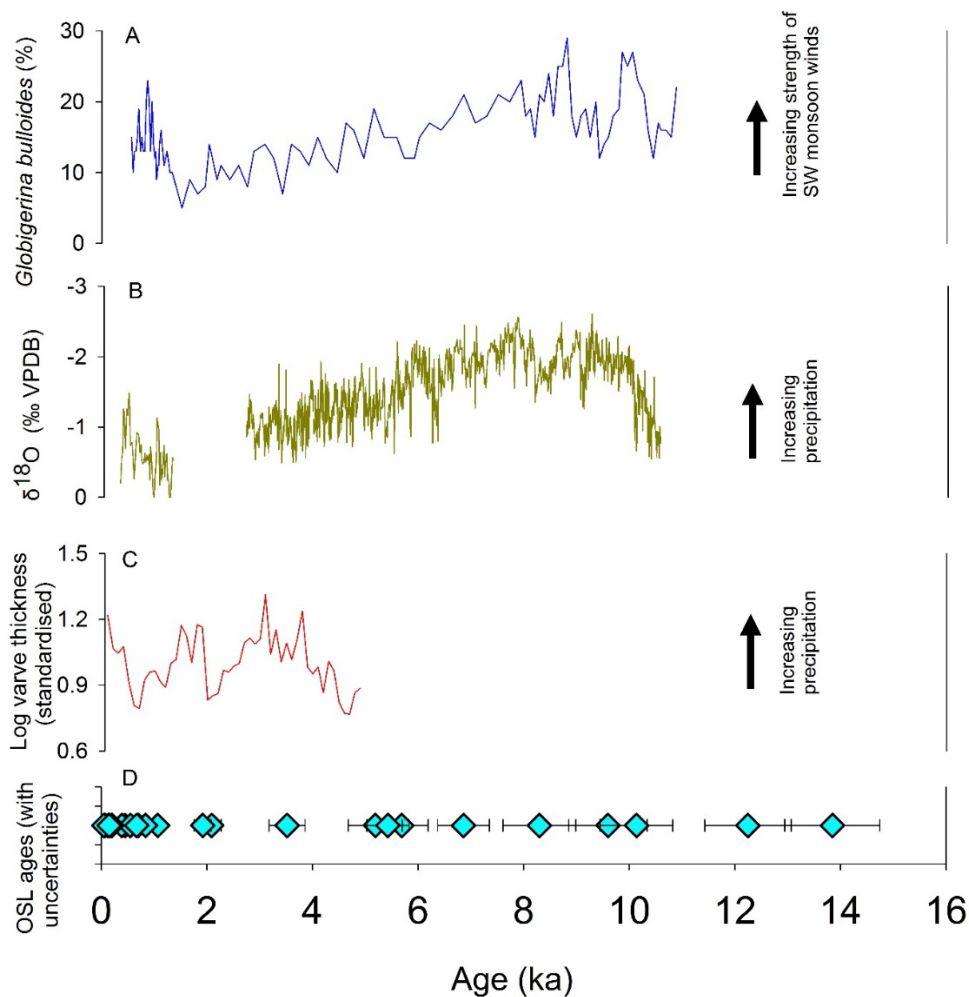


Figure 8. (A) *G. bulloides* percentage from core ODP 723 A core off Oman coast in the Arabian Sea, as a proxy for SW Monsoon wind strength (Gupta et al., 2003). (B) Oxygen-isotope record from a stalagmite in Qunf, southern Oman reflecting as a proxy of monsoon precipitation for the periods 10.3-2.7 ka and

1 **1.4-0.4 ka (Fleitmann et al., 2003). (C) A reconstruction of annually laminated**
2 **(varved) marine sediment thickness record from cores SO 90 39KG/56KA, NE**
3 **Arabian Sea, as a proxy for monsoon precipitation (von Rad et al., 1999). (D)**
4 **The OSL ages and uncertainties calculated in this study.**

6 **4.2 Implications for the timing and evolution of parabolic dunes**

7 Parabolic dunes tend to form in partially vegetated aeolian landscapes and are
8 sensitive to both environmental and human controls. The formation, development and
9 morphology of parabolic dunes involve complex interactions between an initial surface
10 blowout, the strength and directional variability of the wind, the source and amount of
11 sand involved, the density and type of vegetation, and salinity and levels of
12 groundwater (Pye and Tsoar, 1990; Nield and Baas, 2008; Hugenholtz and Wolfe,
13 2006; Langford et al., 2009). Under deteriorating vegetation cover conditions and
14 anthropogenic disturbances, parabolic dunes can transform to more mobile, non-
15 parabolic dunes (e.g. Hack, 1941; Anton and Vincent, 1986; Hesp, 2001). Once
16 reactivated, the mobility of these dunes may last for decades or centuries depending
17 upon the wind energy in the arid environments (Bullard et al., 1997; Hugenholtz and
18 Wolfe 2005).

19 In the study region, dune reactivation in recent times and subsequent aeolian
20 accumulation has led to the multi-generational development of parabolic dunes. The
21 luminescence chronology presented shows that the parabolic dunes in the region
22 accumulated during late Pleistocene-Early Holocene. The parallelism of dune arms
23 implies prevailing winds have been unidirectional since their accumulation (e.g.
24 Wasson et al., 1983). Modern disturbances linked to land use pressures have resulted
25 in the reactivation of sand dunes and this has resulted in formations of new crescentic
26 features atop parabolic dunes (Figure 9), which Wadhawan (1998) described as
27 products of low energy flows. These superimposed features show migratory
28 characteristics (Figure 9) in the way that they propagate further downwind, presenting
29 an advancement of the bedform, and producing sets of weak laminations, which are
30 observed on the top of all the sampled dune sites (Figure 2C, inset). The quantification
31 of the migratory trait is hampered by a Government restriction on access to aerial
32 photography however, the luminescence chronology confirms that these
33 superimposed features are episodic and young in nature. At Setrawa dune site, large
34 aliquots from two samples collected from a dune arm (at 2.5 m and 7.5 m respectively)
35 650 m away from the nose, generated very low, indiscernible OSL signals and
36 therefore demonstrate that these superimposed features have been deposited very
37 recently. This was also the case at Tinwari, where two samples collected from a dune
38 arm (at 1 m and 2 m depth) 500 m from the dune nose were accumulated less than
39 150 years ago (Thar 18/1/2 and Thar 18/1/4). The absence of older ages at such
40 depths from these arms not only shows evidence of a large scale recent reactivation,
41 but also suggests that these migratory superimposed features are depositing sand
42 near the nose of the dunes. As a result, the sets of parabolic dunes are developing
43 high transverse wall-like features (C↔D, Figure 10), which act as major zone of
44 accumulation. The OSL ages show rapid net accumulation in recent times on the top

half of these wall-like features, resting unconformably on the top of older, stabilised aeolian deposits. Such features are similar to the barchanoid-parabolic transitional dunes described recently by Yan and Baas (2017) using simulation results from the Extended-DECAL (Discrete Eco-geomorphic Aeolian Landscapes model of Nield and Baas (2008) and Baas and Nield (2010) and empirical data from fieldwork in Inner Mongolia, China. Although the transition of parabolic dunes to other dune types has been observed in various dune systems around the world (Pye and Tsoar, 1990), there have been very little investigation of them; the majority of which are based on aerial photographs (Yan and Baas, 2015). This study from a parabolic dunefield in the Thar presents OSL dating as a powerful chronometric tool to understand geomorphic transformations of dunes over longer time scales.

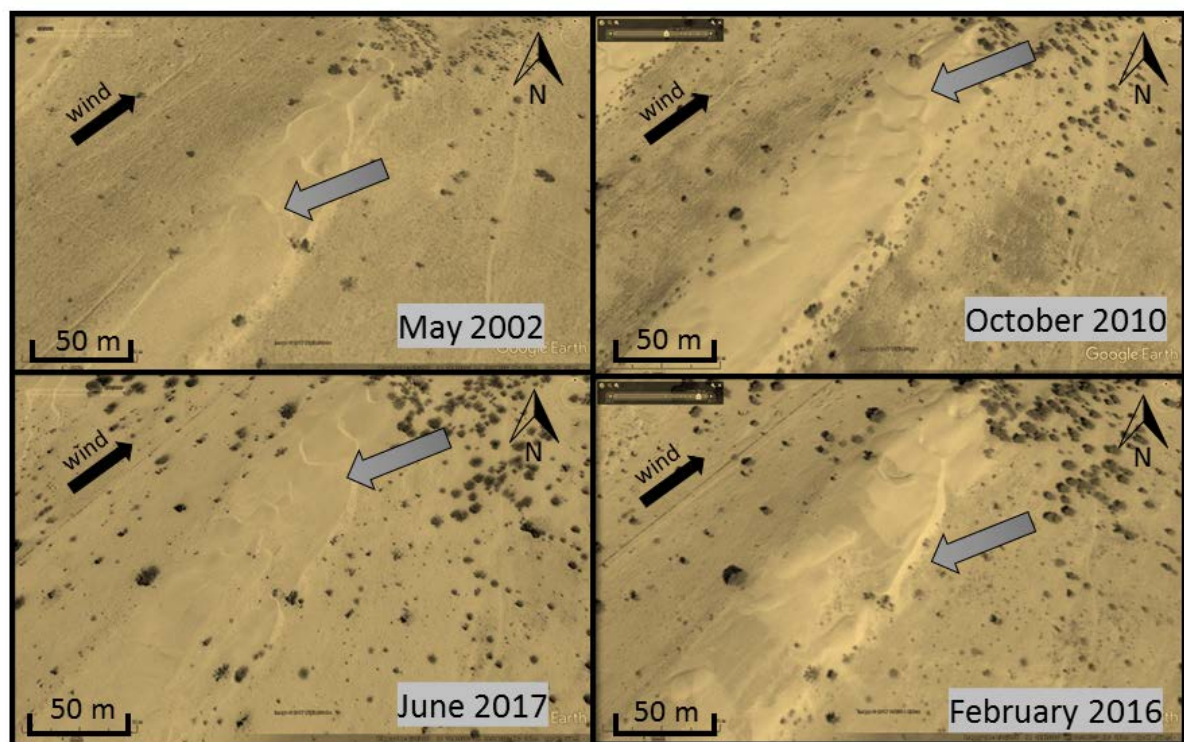


Figure 9. Meso-scale ephemeral transverse accretionary dune forms forming on the top of a parabolic dune arm in Dechu. The grey arrows point at their forward propagation over the past 15 years (clockwise). Satellite imagery courtesy of 2018 Google Earth Pro© 2018.

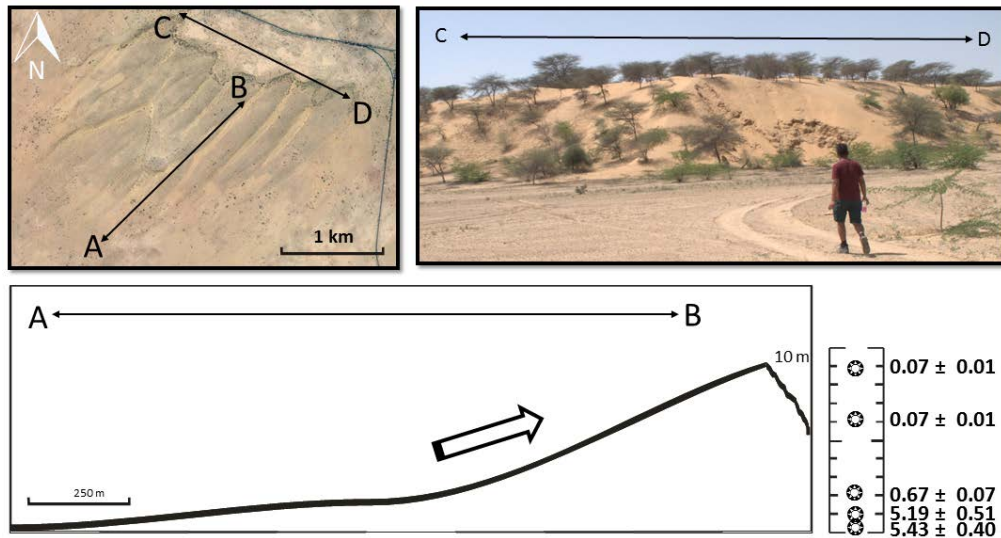


Figure 10. The NW-SE alignment of the transverse wall-like feature (C↔D) and their forepart appearance at Dechu (Thar 16/10). Note, the rapid ~4 m dune accumulation in last 70 years in the downwind direction.

5 Conclusions

This study has presented a new history of desert dune accumulation in the eastern-central Thar Desert by applying OSL dating to a series of intensively sampled sections through dune sedimentary bodies. We demonstrate that the development of dunes in this region has been both more complex and more recent than previous investigations have suggested. The main parabolic dunefield present today is largely a function of late Pleistocene-early Holocene dune accumulation, which is significantly more recent than the previous chronologies presented by Singhvi and Kar (2004) and Dhir et al. (2010). Furthermore, there is a strong record of dune activity and disturbance in recent millennia and centuries, particularly during the last 70 years when a significantly expanded human presence in the landscape coincides with the widespread disturbance of dune surfaces and the development of superimposed transverse bedforms. These new bedforms seem to favour the formation of wall-like transverse features downwind.

The history of the Thar Desert dune landscape demonstrates the interplay of natural and anthropogenic processes in landscape development, and the susceptibility of this marginally arid region to land use pressures today. Other dune systems within this extensive desert region may reveal differing aeolian histories, but this study has shown that a strategic approach to sampling allows the scope for a more complex chronology to be identified and subsequently enhance our understanding of dune development.

6 Acknowledgements

The doctoral studies of the first author are funded by Clarendon Scholarship, University of Oxford. The authors thank the John Fell Fund, University of Oxford (Grant Number 132/062) for providing funding for fieldwork and laboratory analyses. The first author thanks Dr. Szilvia Bajkan for her assistance in the laboratory. He also thanks the Quaternary Research Association for supporting attendance at the 9th International Conference on Geomorphology in New Delhi (2017), where this work was initially presented. We thank the anonymous reviewers for their comments and suggestions.

References

- ANTON, D.J. and VINCENT, P., 1986. Parabolic dunes of the Jafurah desert, eastern province, Saudi Arabia. *Journal of arid environments*, 11.
- ARNOLD, L.J. and ROBERTS, R.G., 2009. Stochastic modelling of multi-grain equivalent dose (De) distributions: implications for OSL dating of sediment mixtures. *Quaternary Geochronology*, 4(3), pp. 204-230.
- ATKINSON, O.A., THOMAS, D.S., GOUDIE, A.S. and BAILEY, R.M., 2011. Late Quaternary chronology of major dune ridge development in the northeast Rub'al-Khali, United Arab Emirates. *Quaternary Research*, 76(1), pp. 93-105.
- BAAS, A.C. and NIELD, J.M., 2010. Ecogeomorphic state variables and phase-space construction for quantifying the evolution of vegetated aeolian landscapes. *Earth Surface Processes and Landforms: The Journal of the British Geomorphological Research Group*, 35(6), pp.717-731.
- BAILEY, R. M., and D. S. G. THOMAS. "A quantitative approach to understanding dated dune stratigraphies." *Earth Surface Processes and Landforms* 39.5 (2014): 614-631.
- BANERJEE, D., MURRAY, A.S., BØTTER-JENSEN, L. and LANG, A., 2001. Equivalent dose estimation using a single aliquot of polymineral fine grains. *Radiation Measurements*, 33(1), pp. 73-94.
- BATEMAN, M.D., BOULTER, C.H., CARR, A.S., FREDERICK, C.D., PETER, D. and WILDER, M., 2007. Detecting post-depositional sediment disturbance in sandy deposits using optical luminescence. *Quaternary geochronology*, 2(1-4), pp. 57-64.
- BELL, W., 1979. Attenuation factors for the absorbed radiation dose in quartz inclusions for thermoluminescence dating. *Ancient TL*, 8(2), pp. 12.
- BELL, W., 1979. Attenuation factors for the absorbed radiation dose in quartz inclusions for thermoluminescence dating. *Ancient TL*, 8(2), pp. 12.
- BLOTT, S., 2000. GRADISTAT Version 4.0: A grain size distribution and statistics package for the analysis of unconsolidated sediments by sieving or laser granulometer. URL: http://www.kpal.co.uk/gradistat_abstract.htm, .

- 1 BØTTER-JENSEN, L., ANDERSEN, C., DULLER, G.A. and MURRAY, A.S., 2003.
2 Developments in radiation, stimulation and observation facilities in luminescence
3 measurements. *Radiation Measurements*, **37**(4-5), pp. 535-541.
- 4 BRYSON, A. A. and BARREIS, D., Possibilities of major climatic modifications and
5 their implications: Northwest India, A case study. *Bull. Am. Meteorol. Soc.*, 1967, 48,
6 136–142.
- 7 BULLARD, J., THOMAS, D., LIVINGSTONE, I. and WIGGS, G., 1997. Dunefield
8 activity and interactions with climatic variability in the southwest Kalahari Desert. *Earth*
9 *Surface Processes and Landforms*, **22**(2), pp. 165-174.
- 10 CHAWLA, S., DHIR, R. and SINGHVI, A., 1992. Thermoluminescence chronology of
11 sand profiles in the Thar Desert and their implications. *Quaternary Science*
12 *Reviews*, **11**(1-2), pp. 25-32.
- 13 DIETZE, M., KREUTZER, S., BUROW, C., FUCHS, M.C., FISCHER, M. and
14 SCHMIDT, C., 2016. The abanico plot: visualising chronometric data with individual
15 standard errors. *Quaternary Geochronology*, **31**, pp. 12-18.
- 16 DHIR, R., SINGHVI, A., ANDREWS, J., KAR, A., SAREEN, B., TANDON, S.,
17 KAILATH, A. and THOMAS, J., 2010. Multiple episodes of aggradation and calcrete
18 formation in Late Quaternary aeolian sands, Central Thar Desert, Rajasthan,
19 India. *Journal of Asian Earth Sciences*, **37**(1), pp. 10-16.
- 20 DULLER, G.A.T., 2003. Distinguishing quartz and feldspar in single grain
21 luminescence measurements. *Radiation Measurements*, **37**(2), pp. 161-165.
- 22 DULLER, G.A.T., 2008. Single-grain optical dating of Quaternary sediments: why
23 aliquot size matters in luminescence dating. *Boreas*, **37**(4), pp. 589-612.
- 24 DURCAN, J.A. and DULLER, G.A.T., 2011. The fast ratio: a rapid measure for testing
25 the dominance of the fast component in the initial OSL signal from quartz. *Radiation*
26 *Measurements*, **46**(10), pp. 1065-1072.
- 27 DURCAN, J.A., KING, G.E. and DULLER, G.A.T., 2015. DRAC: Dose Rate and Age
28 Calculator for trapped charge dating. *Quaternary Geochronology*, **28**, pp. 54-61.
- 29 DURCAN, J.A., THOMAS, D.S., GUPTA, S., PAWAR, V., SINGH, R.N. and PETRIE,
30 C.A., 2017. Holocene landscape dynamics in the Ghaggar-Hakra palaeochannel
31 region at the northern edge of the Thar Desert, northwest India. *Quaternary*
32 *International*.
- 33 FLEITMANN, D., BURNS, S.J., MUDELSEE, M., NEFF, U., KRAMERS, J., MANGINI,
34 A. AND MATTER, A., 2003. Holocene forcing of the Indian monsoon recorded in a
35 stalagmite from southern Oman. *Science*, 300(5626), pp.1737-1739.
- 36 FITZSIMMONS, K.E., RHODES, E.J., MAGEE, J.W. and BARROWS, T.T., 2007. The
37 timing of linear dune activity in the Strzelecki and Tirari Deserts, Australia. *Quaternary*
38 *Science Reviews*, **26**(19-21), pp. 2598-2616.

- 1 FOLK, R.L. and WARD, W.C., 1957. Brazos River bar: a study in the significance of
2 grain size parameters. *Journal of Sedimentary Research*, **27**(1).
- 3 GALBRAITH, R.F., ROBERTS, R.G., LASLETT, G.M., YOSHIDA, H. and OLLEY,
4 J.M., 1999. Optical dating of single and multiple grains of quartz from Jinmium rock
5 shelter, northern Australia: Part I, experimental design and statistical
6 models. *Archaeometry*, **41**(2), pp. 339-364.
- 7 GIOSAN, L., CLIFT, P.D., MACKLIN, M.G., FULLER, D.Q., CONSTANTINESCU, S.,
8 DURCAN, J.A., STEVENS, T., DULLER, G.A.T., TABREZ, A.R., GANGAL, K.,
9 ADHIKARI, R., ALIZAI, A., FILIP, F., VANLANINGHAM, S. and SYVITSKI, J.P., 2012.
10 Fluvial landscapes of the Harappan civilization. *Proceedings of the National Academy
11 of Sciences of the United States of America*, **109**(26), pp. E1688-94.
- 12 GUÉRIN, G., MERCIER, N. and ADAMIEC, G., 2011. Dose-rate conversion factors:
13 update. *Ancient TL*, **29**(1), pp. 5-8.
- 14 GUÉRIN, G., MERCIER, N., NATHAN, R., ADAMIEC, G. and LEFRAIS, Y., 2012. On
15 the use of the infinite matrix assumption and associated concepts: a critical
16 review. *Radiation Measurements*, **47**(9), pp. 778-785.
- 17 GUPTA, A.K., ANDERSON, D.M. and OVERPECK, J.T., 2003. Abrupt changes in the
18 Asian southwest monsoon during the Holocene and their links to the North Atlantic
19 Ocean. *Nature*, **421**(6921), pp. 354.
- 20 HACK, J.T., 1941. Dunes of the western Navajo country. *Geographical Review*, **31**(2),
21 pp.240-263.
- 22 HEER, A.J., ADAMIEC, G. and MOSKA, P., 2012. How many grains are there on a
23 single aliquot? *Ancient TL*, **30**(1), pp. 9-11.
- 24 HEIRI, O., LOTTER, A.F. and LEMCKE, G., 2001. Loss on ignition as a method for
25 estimating organic and carbonate content in sediments: reproducibility and
26 comparability of results. *Journal of Paleolimnology*, **25**(1), pp. 101-110.
- 27 HESP, P., 2011. 3.08 Dune Coasts. *Treatise on Estuarine and Coastal Science*.
28 Academic Press, Waltham, pp.193-221.
- 29 HUGENHOLTZ, C.H. and WOLFE, S.A., 2006. Morphodynamics and climate controls
30 of two aeolian blowouts on the northern Great Plains, Canada. *Earth Surface
31 Processes and Landforms*, **31**(12), pp. 1540-1557.
- 32 HUGENHOLTZ, C.H. and WOLFE, S.A., 2005. Recent stabilization of active sand
33 dunes on the Canadian prairies and relation to recent climate
34 variations. *Geomorphology*, **68**(1-2), pp. 131-147.
- 35 JACOBS, Z., DULLER, G.A.T., WINTLE, A.G. and HENSHILWOOD, C.S., 2006.
36 Extending the chronology of deposits at Blombos Cave, South Africa, back to 140 ka
37 using optical dating of single and multiple grains of quartz. *Journal of human
38 evolution*, **51**(3), pp. 255-273.

- 1 JUYAL, N., CHAMYAL, L., BHANDARI, S., BHUSHAN, R. and SINGHVI, A., 2006.
2 Continental record of the southwest monsoon during the last 130 ka: evidence from
3 the southern margin of the Thar Desert, India. *Quaternary Science Reviews*, **25**(19-
4 20), pp. 2632-2650.
- 5 KAR, A., 1993. Aeolian processes and bedforms in the Thar Desert. *Journal of Arid*
6 *Environments*, **25**(1), pp. 83-96.
- 7 KAR, A., 2013. Quaternary geomorphic processes and landform development in the
8 Thar Desert of Rajasthan. *Landforms Processes and Environment Management*, pp.
9 225-256.
- 10 KAR, A., FELIX, C., RAJAGURU, S. and SINGHVI, A., 1998. Late Holocene growth
11 and mobility of a transverse dune in the Thar Desert. *Journal of Arid*
12 *Environments*, **38**(2), pp. 175-185.
- 13 KAR, A., MOHRANA, P., RAINA, P., KUMAR, M., SONI, M., SANTRA, P., ARYA, A.A.
14 and DHINWA, P., 2009. Desertification and its control measures. *Trends in Arid Zone*
15 *Research in India*, pp. 1-47.
- 16 KAR, A., SINGHVI, A., JUYAL, N. and RAJAGURU, S., 2004. Late Quaternary aeolian
17 sedimentation history of the Thar Desert. *Geomorphology and Environment*, pp. 105-
18 122.
- 19 KISS, T., SIPOS, G. and KOVÁCS, F., 2009. Human impact on fixed sand dunes
20 revealed by morphometric analysis. *Earth Surface Processes and Landforms*, **34**(5),
21 pp. 700-711.
- 22 KREUTZER, S., DIETZE, M., BUROW, C., FUCHS, M., SCHMIDT, C., FISCHER, M.
23 and FRIEDRICH, J., 2017. *Luminescence: Comprehensive Luminescence Dating*
24 *Data Analysis.R package version 0.7.3*,
- 25 LANCASTER, N., WOLFE, S., THOMAS, D., BRISTOW, C., BUBENZER, O.,
26 BURROUGH, S., DULLER, G.A.T., HALFEN, A., HESSE, P. and ROSKIN, J., 2016.
27 The INQUA dunes atlas chronologic database. *Quaternary International*, **410**, pp. 3-
28 10.
- 29 LANGFORD, R.P., ROSE, J.M. and WHITE, D.E., 2009. Groundwater salinity as a
30 control on development of eolian landscape: An example from the White Sands of
31 New Mexico. *Geomorphology*, **105**(1-2), pp. 39-49.
- 32 LEIGHTON, C.L., BAILEY, R.M. and THOMAS, D.S., 2013. The utility of desert sand
33 dunes as Quaternary chronostratigraphic archives: evidence from the northeast Rub'al
34 Khali. *Quaternary Science Reviews*, **78**, pp. 303-318.
- 35 MOHARANA, P.C., GAUR, M.K., CHAUDHARY, C., CHAUHAN, J.S. and
36 RAJPUROHIT, R.S., 2013. A system of geomorphological mapping for western
37 Rajasthan with relevance for agricultural land use. *Annals of Arid Zone*, **52**(3&4),
38 pp.163-180.

- 1 MURRAY, A.S. and WINTLE, A.G., 2003. The single aliquot regenerative dose
2 protocol: potential for improvements in reliability. *Radiation Measurements*, **37**(4-5),
3 pp. 377-381.
- 4 MURRAY, A.S. and WINTLE, A.G., 2000. Luminescence dating of quartz using an
5 improved single-aliquot regenerative-dose protocol. *Radiation Measurements*, **32**(1),
6 pp. 57-73.
- 7 NATHAN, R., THOMAS, P., JAIN, M., MURRAY, A. and RHODES, E., 2003.
8 Environmental dose rate heterogeneity of beta radiation and its implications for
9 luminescence dating: Monte Carlo modelling and experimental validation. *Radiation*
10 *Measurements*, **37**(4-5), pp. 305-313.
- 11 NIELD, J.M. and BAAS, A.C., 2008. The influence of different environmental and
12 climatic conditions on vegetated aeolian dune landscape development and
13 response. *Global and Planetary Change*, **64**(1-2), pp. 76-92.
- 14 OLLEY, J.M., PIETSCH, T. and ROBERTS, R.G., 2004. Optical dating of Holocene
15 sediments from a variety of geomorphic settings using single grains of
16 quartz. *Geomorphology*, **60**(3-4), pp. 337-358.
- 17 PIGGOTT, STUART. 1950. Prehistoric India to 1000 B.C. (Penguin Books).
18 Harmondsworth.
- 19 PRASAD, S. and ENZEL, Y., 2006. Holocene paleoclimates of India. *Quaternary*
20 *Research*, **66**(3), pp. 442-453.
- 21 PRESCOTT, J.R. and HUTTON, J.T., 1994. Cosmic ray contributions to dose rates
22 for luminescence and ESR dating: large depths and long-term time
23 variations. *Radiation Measurements*, **23**(2-3), pp. 497-500.
- 24 PYE, K. and TSOAR, H., 1990. 1990: Aeolian sand and sand dunes. London: Unwin
25 Hyman. .
- 26 RODELL, M., VELICOGNA, I. and FAMIGLIETTI, J.S., 2009. Satellite-based
27 estimates of groundwater depletion in India. *Nature*, **460**(7258), pp. 999.
- 28 ROY, P., NAGAR, Y., JUYAL, N., SMYKATZ-KLOSS, W. and SINGHVI, A., 2009.
29 Geochemical signatures of Late Holocene paleo-hydrological changes from Phulera
30 and Pokharan saline playas near the eastern and western margins of the Thar Desert,
31 India. *Journal of Asian Earth Sciences*, **34**(3), pp. 275-286.
- 32 SAINI, H. and MUJTABA, S., 2012. Depositional history and palaeoclimatic variations
33 at the northeastern fringe of Thar Desert, Haryana Plains, India. *Quaternary*
34 *international*, **250**, pp. 37-48.
- 35 SAINI, H., TANDON, S., MUJTABA, S., PANT, N. and KHORANA, R., 2009.
36 Reconstruction of buried channel-floodplain systems of the northwestern Haryana
37 Plains. *Current science*, **97**(11),

- 1 SHITAOKA, Y., MAEMOKU, H. and NAGATOMO, T., 2012. Quartz OSL dating of
2 sand dunes in Ghaggar Basin, northwestern India. *Geochronometria*, **39**(3), pp. 221-
3 226.
- 4 SINGHVI, A., BANERJEE, D., RAJAGURU, S. and KUMAR, V.K., 1994.
5 Luminescence chronology of a fossil dune at Budha Pushkar, Thar Desert:
6 Palaeoenvironmental and archaeological implications. *Current science*, pp. 770-773.
- 7 SINGHVI, A.K. and KAR, A., 2004. The aeolian sedimentation record of the Thar
8 Desert. *Journal of Earth System Science*, **113**(3), pp. 371-401.
- 9 SINGHVI, A., SHARMA, Y. and AGRAWAL, D., 1982. Thermoluminescence dating of
10 sand dunes in Rajasthan, India. *Nature*, **295**(5847), pp. 313.
- 11 STOKES, S., 1994. Optical dating of selected Late Quaternary aeolian sediments from
12 Western United States, D. Phil Thesis, University of Oxford.
- 13 STONE, A. and THOMAS, D., 2008. Linear dune accumulation chronologies from the
14 southwest Kalahari, Namibia: challenges of reconstructing late Quaternary
15 palaeoenvironments from aeolian landforms. *Quaternary Science Reviews*, **27**(17-
16 18), pp. 1667-1681.
- 17 THOMAS, J., KAR, A., KAILATH, A., JUYAL, N., RAJAGURU, S. and SINGHVI, A.,
18 1999. Late Pleistocene-Holocene-history of aeolian accumulation in the Thar Desert,
19 India. *ZEITSCHRIFT FUR GEOMORPHOLOGIE SUPPLEMENTBAND*, pp. 181-194.
- 20 VON RAD, U., SCHAAF, M., MICHELS, K.H., SCHULZ, H., BERGER, W.H. and
21 SIROCKO, F., 1999. A 5000-yr record of climate change in varved sediments from the
22 oxygen minimum zone off Pakistan, Northeastern Arabian Sea. *Quaternary*
23 *Research*, **51**(1), pp. 39-53.
- 24 WADHAWAN, S., 1998. Late Quaternary Evolution of Clustered Parabolic Megadunes
25 in Thar Desert, India. *Quaternary Deserts and Climatic Change*, pp. 185-195.
- 26 WASSON, R., RAJAGURU, S., MISRA, V., AGRAWAL, D., DHIR, R., SINGHVI, A.
27 and RAO, K.K., 1983. Geomorphology, late Quaternary stratigraphy and
28 palaeoclimatology of the Thar dunefield. *ZEITSCHRIFT FUR GEOMORPHOLOGIE*
29 *SUPPLEMENTBAND*, **45**, pp. 117-151.
- 30 WINTLE, A.G. and MURRAY, A.S., 2006. A review of quartz optically stimulated
31 luminescence characteristics and their relevance in single-aliquot regeneration dating
32 protocols. *Radiation Measurements*, **41**(4), pp. 369-391.
- 33 YAN, N. and BAAS, A.C., 2015. Parabolic dunes and their transformations under
34 environmental and climatic changes: towards a conceptual framework for
35 understanding and prediction. *Global and Planetary Change*, **124**, pp.123-148.
- 36 YAN, N. and BAAS, A.C., 2017. Environmental controls, morphodynamic processes,
37 and ecogeomorphic interactions of barchan to parabolic dune
38 transformations. *Geomorphology*, **278**, pp.209-237.

- 1 ZHAO, H., LU, Y. and YIN, J., 2007. Optical dating of Holocene sand dune activities
- 2 in the Horqin sand-fields in inner Mongolia, China, using the SAR protocol. *Quaternary*
- 3 *Geochronology*, **2**(1-4), pp. 29-33.

4

5

1 **Table 1. Sedimentology of samples showing Munsell colour, grain size statistics (in microns), organic and carbonate content.**

Sample	Munsell colour	Mean (μm)	Sand (%)				Silt (%)	Clay (%)	Sorting*	Skewness**	Kurtosis***	Organic content (%)	Carbonate content (%)
			Coarse	Medium	Fine	Very Fine							
Thar 16/1/1	10 YR 6/6	185.5	0.0	25.4	64.5	10.1	0.0	0.0	1.478 (MWS)	-0.109 (FS)	1.123 (L)	0.88	0.64
Thar 16/1/2	10 YR 6/4	198.2	0.0	24.2	67.8	7.9	0.0	0.0	1.386 (WS)	-0.001 (S)	0.965 (M)	0.72	0.92
Thar 16/1/4	10 YR 5/4	172.1	0.0	12.3	71.0	16.6	0.0	0.0	1.380 (WS)	-0.002 (S)	0.962 (M)	0.56	0.84
Thar 16/1/5	10 YR 5/4	177.6	0.1	22.6	55.8	14.2	6.8	0.5	1.895 (MS)	-0.300 (FS)	1.844 (VL)	0.84	1.07
Thar 16/1/6	10 YR 5/4	171.9	0.0	20.7	56.5	10.5	11.5	0.8	2.084 (PS)	-0.386 (VFS)	2.255 (VL)	1.54	1.38
Thar 16/1/7	10 YR 5/4	173.8	0.0	21.1	56.8	10.4	10.8	0.8	2.054 (PS)	-0.376 (VFS)	2.238 (VL)	1.15	1.50
Thar 16/1/8	10 YR 6/4	162.3	0.0	10.5	66.5	17.2	5.7	0.1	1.739 (MS)	-0.305 (VFS)	2.077 (VL)	0.92	3.32
Thar 16/1/9	10 YR 6/4	189.4	0.1	25.6	57.8	8.0	8.1	0.4	1.917 (MS)	-0.345 (VFS)	2.186 (VL)	1.15	3.12
Thar 16/3/1	10 YR 7/4	186.9	0.3	26.2	54.5	13.7	5.2	0.0	1.763 (MS)	-0.232 (FS)	1.513 (VL)	0.79	1.10
Thar 16/3/2	10 YR 7/4	152.5	0.0	18.4	51.9	15.0	13.6	1.1	2.287 (PS)	-0.420 (VFS)	2.099 (VL)	1.75	1.82
Thar 16/4/1	10 YR 6/6	229.9	1.1	40.2	54.0	4.7	0.0	0.0	1.446 (MWS)	-0.004 (S)	0.949 (M)	0.69	0.87
Thar 16/4/2	10 YR 6/4	224.4	2.0	38.0	52.4	7.6	0.0	0.0	1.509 (MWS)	0.006 (S)	0.944 (M)	0.53	0.71
Thar 16/4/4	10 YR 6/4	193.6	0.1	24.5	63.7	11.7	0.0	0.0	1.437 (MWS)	0.011 (S)	0.954 (M)	0.62	2.96
Thar 16/4/6	10 YR 6/4	203.3	0.7	31.2	55.2	10.7	2.2	0.0	1.528 (MWS)	-0.030 (S)	0.980 (M)	0.79	0.76
Thar 16/4/7	10 YR 6/4	189.2	0.4	26.9	54.6	9.0	8.2	0.9	2.035 (PS)	-0.340 (VFS)	2.207 (VL)	0.95	1.02
Thar 16/4/8	10 YR 6/4	193.6	0.4	27.3	56.7	9.6	5.5	0.4	1.851 (MS)	-0.285 (FS)	1.923 (VL)	0.79	1.31
Thar 16/4/10	10 YR 6/4	184.3	0.0	20.0	65.8	14.2	0.0	0.0	1.426 (MWS)	0.001 (S)	0.946 (M)	0.66	2.71
Thar 16/6/1	10 YR 5/4	190.2	0.0	23.0	64.4	12.6	0.0	0.0	1.433 (MWS)	0.004 (S)	0.946 (M)	0.78	1.41
Thar 16/6/5	10 YR 5/4	212.7	1.0	35.0	52.8	9.8	1.3	0.0	1.525 (MWS)	-0.039 (S)	0.959 (M)	0.78	1.38
Thar 16/9/1	10 YR 7/4	269.8	5.6	52.0	39.6	1.8	0.9	0.0	1.491 (MWS)	-0.021 (S)	0.951 (M)	0.99	1.33
Thar 16/9/2	10 YR 7/4	197.3	0.1	26.0	63.4	10.5	0.0	0.0	1.430 (MWS)	-0.003 (S)	0.957 (M)	0.68	1.40
Thar 16/9/4	10 YR 7/4	192.0	0.0	23.6	64.3	12.0	0.0	0.0	1.431 (MWS)	--0.002 (S)	0.951 (M)	0.76	1.45
Thar 16/9/5	10 YR 7/4	187.1	0.7	26.2	53.7	15.4	3.9	0.1	1.606 (MWS)	-0.065 (S)	1.045 (M)	0.71	1.44
Thar 16/9/8	10 YR 6/4	168.7	0.2	22.1	52.1	14.1	10.4	1.1	2.194 (PS)	-0.369 (VFS)	2.140 (VL)	1.53	1.48
Thar 16/10/1	10 YR 5/4	200.3	0.0	24.8	68.3	6.9	0.0	0.0	1.374 (WS)	0.001 (S)	0.956 (M)	0.69	1.05
Thar 16/10/4	10 YR 5/4	196.2	0.0	23.1	68.7	8.2	0.0	0.0	1.383 (WS)	0.002 (S)	0.963 (M)	0.71	1.09
Thar 16/10/8	10 YR 5/4	219.2	0.5	35.4	58.6	5.5	0.0	0.0	1.423 (MWS)	0.002 (S)	0.958 (M)	0.61	0.79

Thar 16/10/9	10 YR 5/4	189.0	0.6	27.7	52.1	12.3	6.5	0.2	1.904 (MS)	-0.277 (FS)	1.759 (VL)	0.76	1.00
Thar 16/10/10	10 YR 5/4	183.9	0.1	24.6	56.2	13.0	6.1	0.0	1.806 (MS)	-0.271 (FS)	1.691 (VL)	1.64	1.53
Thar 18/1/2	10 YR 5/4	178.6	0.0	15.0	71.3	13.7	0.0	0.0	0.462 (WS)	0.001 (S)	0.957 (M)	0.46	0.77
Thar 18/1/4	10 YR 5/4	166.5	0.0	8.2	74.9	16.9	0.0	0.0	0.424 (WS)	-0.001 (S)	0.973 (M)	0.54	0.81

* MWS= moderately well sorted, WS= well sorted, MS= moderately sorted, PS= poorly sorted.

** FS= finely skewed, VFS= very finely skewed, S= symmetrical.

*** L= leptokurtic, VL= very leptokurtic, M= mesokurtic.

Table 2. Summary OSL data. Equivalent doses (D_e), dose rates (\dot{D}), and ages are shown to two decimal places, with all calculations made prior to rounding. All dates are relative to the year 2018. D_e s were measured from small aliquots of sample with the exception of Thar 16/4/1 and 16/4/2 (medium aliquots) and Thar 16/4/10 (large aliquots).

Sample	Depth (m)	Discs accepted (measured)	Over- dispersion (%)	CAM D_e (Gy)	Beta \dot{D} (Gy.ka ⁻¹)	Gamma \dot{D} (Gy.ka ⁻¹)	Cosmic \dot{D} (Gy.ka ⁻¹)	Envir \dot{D} (Gy.ka ⁻¹)	Age (ka)
Thar 16/1/1	0.5	20 (28)	47.2 ± 8.1	0.90 ± 0.10	1.17 ± 0.11	0.62 ± 0.04	0.21 ± 0.02	2.00 ± 0.12	0.45 ± 0.06
Thar 16/1/2	0.7	25 (32)	19.2 ± 3.7	0.88 ± 0.06	1.28 ± 0.11	0.81 ± 0.05	0.19 ± 0.01	2.28 ± 0.12	0.39 ± 0.03
Thar 16/1/4	6.0	28 (46)	28.7 ± 4.3	1.18 ± 0.07	1.25 ± 0.11	0.78 ± 0.05	0.10 ± 0.01	2.14 ± 0.12	0.55 ± 0.05
Thar 16/1/5	14.0	22 (48)	28.9 ± 4.5	2.38 ± 0.15	1.34 ± 0.12	0.83 ± 0.06	0.05 ± 0.01	2.22 ± 0.13	1.07 ± 0.09
Thar 16/1/6	20.0	37 (48)	24.1 ± 2.9	14.31 ± 0.58	1.27 ± 0.11	0.78 ± 0.05	0.03 ± 0.00	2.09 ± 0.12	6.86 ± 0.49
Thar 16/1/7	21.0	27 (38)	30.0 ± 4.1	17.21 ± 1.01	1.27 ± 0.11	0.78 ± 0.05	0.03 ± 0.00	2.07 ± 0.12	8.30 ± 0.69
Thar 16/1/8	22.0	22 (38)	25.1 ± 3.9	20.71 ± 1.13	1.27 ± 0.10	0.86 ± 0.06	0.03 ± 0.00	2.16 ± 0.12	9.60 ± 0.74
Thar 16/1/9	23.0	30 (42)	28.6 ± 3.8	22.70 ± 1.26	1.01 ± 0.09	0.61 ± 0.04	0.03 ± 0.00	1.64 ± 0.10	13.85 ± 1.11
Thar 16/3/1	11.0	20 (44)	39.7 ± 8.4	1.60 ± 0.17	1.39 ± 0.12	0.88 ± 0.06	0.07 ± 0.01	2.34 ± 0.13	0.68 ± 0.08

Thar 16/3/2	19	20 (29)	29.3 ± 4.8	12.07 ± 0.82	1.27 ± 0.11	0.82 ± 0.06	0.03 ± 0.00	2.12 ± 0.12	5.69 ± 0.50
Thar 16/4/1	0.3	20 (42)	63.4 ± 16.0	0.44 ± 0.09	1.17 ± 0.10	0.77 ± 0.05	0.22 ± 0.02	2.16 ± 0.11	0.20 ± 0.03
Thar16/4/2	1.0	20 (45)	22.7 ± 13.7	0.36 ± 0.08	1.33 ± 0.12	0.75 ± 0.05	0.18 ± 0.02	2.26 ± 0.13	0.16 ± 0.03
Thar 16/4/4	2.0	25 (32)	31.9 ± 4.9	1.89 ± 0.13	1.31 ± 0.11	0.78 ± 0.05	0.16 ± 0.02	2.24 ± 0.13	0.84 ± 0.08
Thar 16/4/6	5.0	21 (30)	30.2 ± 4.7	4.67 ± 0.31	1.32 ± 0.11	0.80 ± 0.05	0.11 ± 0.01	2.23 ± 0.13	2.09 ± 0.18
Thar 16/4/7	6.0	24 (45)	26.5 ± 4.3	4.47 ± 0.26	1.37 ± 0.12	0.85 ± 0.06	0.10 ± 0.01	2.33 ± 0.13	1.92 ± 0.16
Thar 16/4/8	7.0	27 (38)	20.2 ± 2.9	22.84 ± 0.91	1.31 ± 0.11	0.85 ± 0.06	0.09 ± 0.01	2.25 ± 0.13	10.14 ± 0.69
Thar 16/4/10	9.0	31 (52)	19.1 ± 2.7	23.03 ± 0.84	1.12 ± 0.10	0.69 ± 0.05	0.08 ± 0.01	1.88 ± 0.11	12.25 ± 0.82
Thar 16/6/1	0.5	21 (68)	62.5 ± 16.0	0.16 ± 0.03	1.18 ± 0.10	0.82 ± 0.06	0.21 ± 0.02	2.20 ± 0.11	0.07 ± 0.01
Thar 16/6/5	5.0	22 (52)	72.0 ± 14.5	0.15 ± 0.03	1.30 ± 0.11	0.77 ± 0.05	0.11 ± 0.01	2.18 ± 0.13	0.07 ± 0.01
Thar 16/9/1	1.5	20 (32)	39.3 ± 10.3	0.16 ± 0.02	1.25 ± 0.10	0.91 ± 0.06	0.17 ± 0.02	2.33 ± 0.12	0.07 ± 0.01
Thar 16/9/2	2.5	26 (35)	64.1 ± 12.1	0.18 ± 0.03	1.90 ± 0.16	1.19 ± 0.08	0.15 ± 0.02	3.24 ± 0.18	0.06 ± 0.01
Thar 16/9/4	4.5	21 (37)	55.1 ± 9.3	0.24 ± 0.03	0.97 ± 0.08	0.67 ± 0.05	0.12 ± 0.01	1.76 ± 0.09	0.14 ± 0.02
Thar 16/9/5	5.5	21 (29)	31.8 ± 6.1	0.31 ± 0.02	1.36 ± 0.12	0.84 ± 0.06	0.11 ± 0.01	2.31 ± 0.13	0.13 ± 0.01
Thar 16/9/8	8.5	25 (52)	37.6 ± 5.6	7.65 ± 0.61	1.24 ± 0.10	0.85 ± 0.06	0.08 ± 0.01	2.18 ± 0.12	3.52 ± 0.34
Thar 16/10/1	1.0	22 (50)	25.8 ± 9.6	0.15 ± 0.01	1.13 ± 0.09	0.75 ± 0.05	0.18 ± 0.02	2.06 ± 0.11	0.07 ± 0.01
Thar 16/10/4	3.7	26 (50)	61.0 ± 12.3	0.15 ± 0.02	1.27 ± 0.11	0.74 ± 0.05	0.13 ± 0.01	2.14 ± 0.12	0.07 ± 0.01
Thar 16/10/8	8.2	21 (50)	35.5 ± 6.7	1.58 ± 0.14	1.36 ± 0.11	0.92 ± 0.06	0.08 ± 0.01	2.36 ± 0.13	0.67 ± 0.07
Thar 16/10/9	9.2	20 (26)	28.8 ± 4.8	12.80 ± 1.04	1.42 ± 0.12	0.97 ± 0.07	0.07 ± 0.01	2.47 ± 0.13	5.19 ± 0.51
Thar 16/10/10	10.2	30 (64)	26.2 ± 3.7	11.45 ± 0.56	1.23 ± 0.10	0.81 ± 0.05	0.07 ± 0.01	2.11 ± 0.12	5.43 ± 0.40
Thar 18/1/2	1.0	23 (30)	73.6 ± 13.5	0.11 ± 0.02	1.33 ± 0.12	0.79 ± 0.05	0.18 ± 0.02	2.30 ± 0.13	0.05 ± 0.01
Thar18/1/4	2.0	22 (26)	76.2 ± 12.1	0.35 ± 0.06	1.31 ± 0.11	0.89 ± 0.06	0.16 ± 0.02	2.36 ± 0.13	0.15 ± 0.03

1

2